

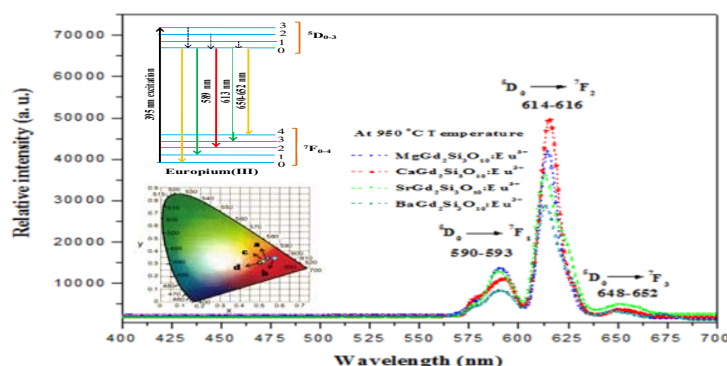
Novel synthesis and Optical investigation of trivalent Europium doped $\text{MGd}_2\text{Si}_3\text{O}_{10}$ ($\text{M} = \text{Mg}^{2+}$, Ca^{2+} , Sr^{2+} and Ba^{2+}) nanophosphors for full-color displays

Suman Sheoran,¹ Sitender Singh,¹ Ajay Mann,² Anura Samantilleke,³ Bernabe Mari,⁴ Devender Singh^{1*}

¹Department of Chemistry, Maharshi Dayanand University, Rohtak 124001, India ²Pt. NRS Government College, Rohtak- 124001, India. ³Centro de Fisica, Universidade of Minho, Braga 4710057, Portugal. ⁴Department de Fisica Aplicada, Universitat Politecnica de Valencia, Valencia 46022, Spain

Submitted on: 20-Aug-2019, Accepted on: 01-Oct-2019 Published on: 07-Oct-2019

ABSTRACT



A series of Eu^{3+} doped $\text{MGd}_2\text{Si}_3\text{O}_{10}$ ($\text{M} = \text{Mg}^{2+}$, Ca^{2+} , Sr^{2+} and Ba^{2+}) was synthesized via sol-gel procedure at 950°C . The optical characteristics of the materials were studied by Photoluminescence (PL) emission spectra. Upon 395 nm excitation and at 0.03 mole concentration of Eu^{3+} ion, these nanophosphors display optimum photoluminescence with most intense peak due to ${}^5\text{D}_0 \rightarrow {}^7\text{F}_2$ (614-616) of dopant. Powder X-ray diffraction (PXRD) analysis proves that all synthesized materials are of crystalline nature and crystallinity improves on increasing temperature. Transmission electron microscopy (TEM) exhibited the spherical shape of particles in 13-30 nm size. Fourier Transformation infrared (FTIR) spectra showed peaks in $400\text{-}1000\text{ cm}^{-1}$ corresponding to gadolinium-oxygen and silicon-oxygen bond vibrations. In $\text{BaGd}_2\text{Si}_3\text{O}_{10}$ material, Gd-O vibration is centered at 492 cm^{-1} and absorption band at 855 cm^{-1} is result of asymmetric vibrations of SiO in silicate tetrahedral unit. Due to excellent photoluminescence and suitable CIE coordinates, these materials could have brilliant applications in innovative displays.

Keywords: $\text{MGd}_2\text{Si}_3\text{O}_{10}$, nanophosphors, displays, lanthanide, luminescence, composites, LED

INTRODUCTION

The rare-earth ions doped phosphor materials have considerably been evaluated for their uses in the advanced display

*Corresponding Author: Dr. Devender Singh
Department of Chemistry, Maharshi Dayanand University, Rohtak
124001, Haryana, India
Tel: +91-9896001262
Email: devjakhhar@gmail.com

Cite as: *J. Mat. NanoSci.*, 2019, 6(2), 73-81.
urn:nbn:sciencein:jmns.2019v6.109

©The ScienceIn ISSN 2394-0867
<http://pubs.thesciencein.org/jmns>

and lighting technology. The phosphors have countless uses in white light emitting devices (WLEDs), cathode ray tubes, lasers, optical communications, vacuum fluorescent display, biological labeling, optoelectronic devices, X-ray imaging, etc.¹⁻⁴ The application of phosphors in the light industry have been manifested due to their characteristic properties like high brightness, lower energy consumption, consistency, low ecological impact, long lifetime and high current density.⁵ The phosphor materials comprise of appropriate host matrix and rare earth ions as a dopant. Upon excitation, host lattice captivates the energy and transfers to activator ion. Such transferred energy is responsible for the excitation of electrons from ground energy level to higher energy levels.⁶⁻⁷ The excited states of these ions

can be populated easily and undergo radiative decay to the lowest energy level causing the phenomenon of luminescence.⁸⁻¹¹ The f-orbitals, deeply embedded in the ions, are protected from the chemical environment and results in sharp emission spectra arising from f-f transitions.¹²⁻¹⁴ The red color is one of the primary constituents for the arena of displays and WLEDs. The synthesis of red phosphors with satisfactory color rendering index and the emission color performance is crucial for the development of optoelectronic materials.¹⁵⁻¹⁷ Recent studies have proved Eu^{3+} ion as the most efficient activator ion, among rare earth ions, for the generation of red color.

Numerous rare-earth and transition metals-based sulfide-phosphors with low voltage have been successively fabricated. Conversely, the sulfide materials are not worthful for optoelectronic devices due to lower thermal and chemical stability and are ecological unfriendly owing to the evolution of sulfide gases under external energy excitation. The stability of different host lattices under external voltage increases in the order as fluorides, sulfides, silicates, garnets and aluminates respectively.¹⁸ Therefore, fabrication of phosphor with high luminous efficacy, high thermal and chemical stability and low energy consumption is pretty challenging.

The phosphor materials have been fabricated with techniques like solid state reaction,¹⁹ microwave heating,²⁰ co-precipitation,²¹ hydrothermal synthesis,²² spray pyrolysis,²³ solution combustion method²⁴ and sol-gel.²⁵ The conservative solid-state process has a plenteous shortcomings comprising very high calcination temperature, time-consuming heating and accumulation of particles.²⁶ Moreover, the crushing route required to decrease the size of the particles leads to a decrease in luminous intensity of samples. Instead, the sol-gel procedure includes the highly uniform mixing of the raw materials to grow the sol, making the assimilation of dopants and co-dopants easy and proficient, in the host lattice through the solution phase. Besides, the gel formed on warming consequences the development of minute pores and all the components of the homogeneous gel get very well mixed. The extremely high surface area of samples outcomes the low temperatures synthesis of the materials.²⁷ The large size particles are not suitable for the application in modern displays bioimaging, coating and optical nano-devices. The phosphor materials having nanosize particles possess suitable electronic and optical properties that make them worthful for the fabrication of optoelectronic materials.

We have tried to imply that the considered lattice, exhibit deep red emission owing to transitions of trivalent europium ion, is appropriate for fabrication of luminescent materials. An efficacious sol-gel procedure was applied to explore these silicate lattice based materials. To assess the color and intensity of these samples, optical investigations have been carried out via Photoluminescence spectroscopy. The prepared samples have also been examined with XRD, FTIR and TEM analysis.

EXPERIMENTAL

MATERIALS AND SYNTHESIS

The powdered samples of Eu^{3+} doped $\text{MGd}_2\text{Si}_3\text{O}_{10}$ ($\text{M} = \text{Mg}^{2+}$, Ca^{2+} , Sr^{2+} and Ba^{2+}) phosphors were produced by sol-gel

technique. $\text{Gd}(\text{NO}_3)_3 \cdot 6\text{H}_2\text{O}$, $\text{Eu}(\text{NO}_3)_3 \cdot 6\text{H}_2\text{O}$, nitrates of alkaline earth metals ($\text{Mg}/\text{Ca}/\text{Sr}/\text{Ba}$) and silica powder were used as precursor component for exploring these luminescent materials.

Initially, $\text{CaGd}_2\text{Si}_3\text{O}_{10}$ phosphor was prepared using 0.01-0.05 moles concentration of Europium(III) ion. For optimum photoluminescence performance, the concentration of Eu^{3+} ion was fixed i.e. 0.03 moles and a series of $\text{CaGd}_2\text{Si}_3\text{O}_{10}$ silicates was synthesized at 950 °C. The synthetic procedure used to develop silicate lattice based materials was consisting of two steps. In first step, 3 moles of silica powder were dissolved in round bottom flask (RBF) containing concentrated nitric acid solution. The smooth gel was formed from solution of RBF on stirring. Alternatively, nitrates of alkaline earth metals [$\text{Mg}/\text{Ca}/\text{Sr}/\text{Ba}$ (1.97 moles) and $\text{Eu}(\text{NO}_3)_3 \cdot 6\text{H}_2\text{O}$ (0.03 moles)] were dissolved (stoichiometric amount) in distilled water in a silica crucible and added the mixture of metal nitrates into the RBF and stirred upto 30 minutes for homogenous mixing. The semi-solid paste was formed from the homogenous mixture of RBF when heated in the silica crucible, on the hot plate. The crucible containing semi-solid paste has been put in muffle furnace preserved at 950 °C for one hour that gave rise to white silicate powders. To examine influence of re-heating on the luminous intensity and crystallinity of materials, the samples were further calcined at the temperatures of 1050 and 1150 °C for one hour. Figure 1 shows the synthetic route for the fabrication of silicate lattice based phosphors.

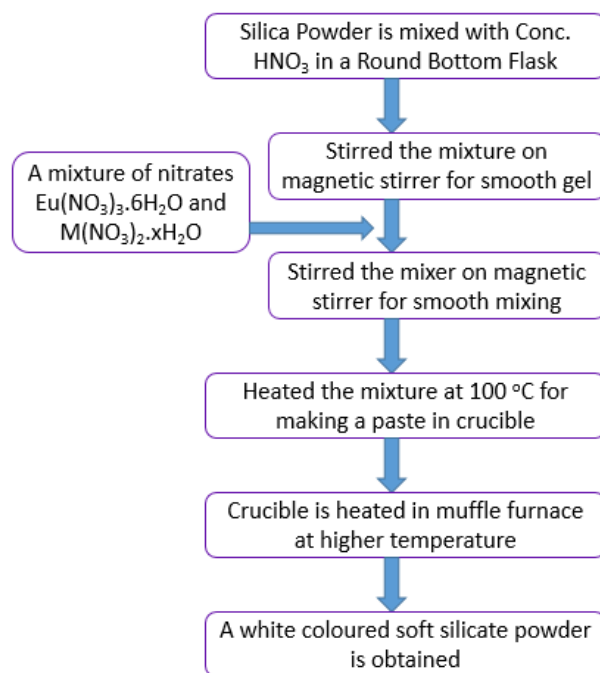


Figure 1. Graphical representation displayed synthetic route of silicate phosphor.

INSTRUMENTATION

For spectroscopic investigations, all the samples were ground in pestle mortar to obtain the powder form and all the examinations were done at room temperature. The optical characteristics of the prepared materials were measured with a xenon lamp (excitation source) assisted Horiba Jobin YVON Fluorolog

spectrophotometer. Photoluminescence spectra of the samples were recorded in 400-700 nm regions. Diffraction studies were made with X-ray diffractometer (Rigaku Ultima IV) using 1.5416 Å wavelength CuK α radiations. X-ray pattern of the materials was recorded from 10°-70° (2 Theta angle) having 4°/min. scanning speed and 0.02° step interval. TECNAI 200 kV (Fei. Electron Optics) TEM was used to evaluate the size of particles of the manufactured silicate phosphors. The chemical environment and arrangement of different elements inside luminescent materials were analyzed from FTIR spectra collected using Bruker Alpha FTIR spectrophotometer.

RESULTS AND DISCUSSIONS

FLUORESCENCE STUDY

The photophysical investigations of the $\text{MgGd}_2\text{Si}_3\text{O}_{10}:\text{Eu}^{3+}$ ($\text{M} = \text{Mg}^{2+}, \text{Ca}^{2+}, \text{Sr}^{2+}$ and Ba^{2+}) crystals have been carried out using UV-visible absorption spectroscopy. The presence of activator ion within the host matrix originates the luminescence.^{28,29} The mechanism of luminescence involves absorption of energy by the host crystal from the external source and the transmission of this absorbed energy to the activator ion. The dopant ion having abundant energy levels undergoes excitation to higher energy levels. Subsequently, it relaxes to the ground level causing the emission of a lesser energy photon that appears as a peak in photoluminescence emission spectra.³⁰ Figure 2 shows the photoluminescent excitation (PLE) spectra of $\text{MgGd}_2\text{Si}_3\text{O}_{10}:\text{Eu}^{3+}$ phosphors at 1150 °C recorded using the PL emission wavelength of 612 nm. PL excitation spectrum is comprises of f-f transitions within the europium(III) ions in the 350 to 550 nm region. The main peaks were detected at 361, 381, 393, 413, 463 and 531 nm owing to the excitation from ${}^7\text{F}_0$ to ${}^5\text{D}_4$, ${}^5\text{L}_7$, ${}^5\text{L}_6$, ${}^5\text{D}_3$, ${}^5\text{D}_2$, and ${}^5\text{D}_1$ in the PLE spectra. The most intense absorption transition was observed at 395 nm (${}^7\text{F}_0 \rightarrow {}^5\text{L}_6$).³¹

The fluorescence spectra of prepared materials were recorded on excitation at 395 nm. The typical photoluminescence emission of $\text{CaGd}_2\text{Si}_3\text{O}_{10}$ prepared using europium ion concentration of 0.01-0.05 moles is depicted in figure 3. The emissive power of $\text{CaGd}_2\text{Si}_3\text{O}_{10}:\text{Eu}^{3+}$ phosphor increases without any change in the spectral shape upon the increase of the concentration of the trivalent europium ion. However, photoluminescent quenching starts as the concentration exceeds 0.03 moles. The increased amount of dopant in the lattice results in an enhanced non-radiative decay, consequently, radiative emission and luminous intensity decrease. The most effective concentration of Eu^{3+} ions in the present matrix is three-mole percent. Hence, the photoluminescence characteristics are susceptible to composition of activator ion in host matrix.^{32,33}

Figure 4a-d depicts the fluorescence spectra of $\text{MgGd}_2\text{Si}_3\text{O}_{10}:\text{Eu}^{3+}$ materials recorded at the absorption wavelength of 395 nm. The red luminescence in Eu^{3+} doped phosphors is the result of incorporation of europium(III) ions within the focused lattice. Such emissions exhibited peaks at 590-593 nm, 614-616 nm and 648-652 nm. These peaks can be attributed to emission from ${}^5\text{D}_0$ electronic state to ${}^7\text{F}_1$, ${}^7\text{F}_2$ and ${}^7\text{F}_3$ transitions respectively.^{34,35} Out of these, ${}^5\text{D}_0 \rightarrow {}^7\text{F}_1$ corresponds to magnetic dipole type of transition and permitted (Judd-Olfelt theory).

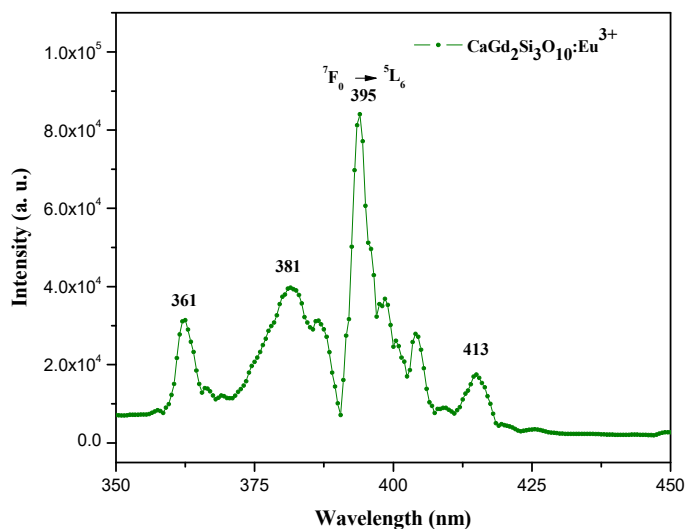


Figure 2. Photoluminescent excitation (PLE) spectra of $\text{CaGd}_2\text{Si}_3\text{O}_{10}$ doped with trivalent europium ion at 1150 °C.

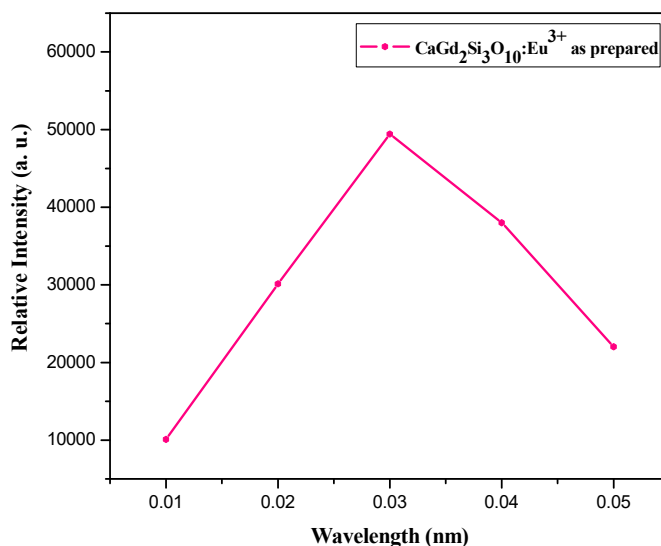


Figure 3. The variation of fluorescent intensity with the concentration of Eu^{3+} ions doped in as prepared $\text{CaGd}_2\text{Si}_3\text{O}_{10}$ phosphor.

However, electric dipole transition (${}^5\text{D}_0 \rightarrow {}^7\text{F}_2$) becomes unusually permitted when the local center of symmetry around the trivalent europium ion is absent. The electrically allowed transition is prevalent over the other two and is responsible for the strong red luminescence in the synthesized materials.³⁶ The high intensity of forced electric dipole transition among the others also tells us about the non-centrosymmetric position of europium(III) site. The intensity of electric dipole transitions has been observed almost 2 to 3 times to that of ${}^5\text{D}_0 \rightarrow {}^7\text{F}_1$, indicating the presence of C_s symmetry around the trivalent europium ion. The lack of inversion symmetry around europium(III) ions provides bright red and efficient phosphors. Relative emission spectrum of these phosphors is also shown in figure 5 indicating that $\text{CaGd}_2\text{Si}_3\text{O}_{10}$ phosphor has maximum luminescence among these prepared materials. Table 1 shows the positions of different peaks, dominant peak and color of the materials under considerations.

These results show that under the synthesis conditions, europium enters the silicate lattice as Eu^{3+} and then substitute Gd^{3+} ion of nearly same size and valence that gives excellent luminescence response applied in white light emitting diode applications. Figure 6 depicts the various possible energy states of trivalent europium ion and transitions proceeding among them.

The intensity of peaks in the spectra is a function of dopant ion concentration. Initially, the luminescence intensity increases with concentration upto an optimum doping concentration and decreases at further higher concentrations. The concentration quenching occurs due to the non-radiative energy transfer between the dopant ions. In $\text{MgGd}_2\text{Si}_3\text{O}_{10}$, the Eu^{3+} ions properly substitute Gd^{3+} ion in the lattice, due to similar charge and comparable ionic radii of Eu^{3+} (95 pm) and Gd^{3+} (94 pm) ions. Therefore, the change in concentration of dopant ion does not significantly affect the structure of crystal lattice.³⁷

The effect of the change in temperature on the luminescence strength of prepared phosphors was also studied by recording the emission at higher temperatures of 1050 and 1150 °C. Emission intensity, in these phosphors, increases with the calcination temperature and maximum photoluminescence response was obtained when prepared phosphors were re-heated at 1150 °C. The increase in luminous intensity on reheating is affected by the

reduced non-radiative (NR) phenomenon at a higher temperature. It is worthwhile to point out that the prepared materials displayed excellent photoluminescence and thermo-stability, even at higher temperature.

The Commission International de l'Eclairage (CIE) values are very important considerations to determine the emissive region for inorganic phosphors having applications in emission devices. Table 2 shows the color coordinates value derived using the photoluminescence emission data of prepared materials, from CIE 1931 color matching functions. Figure 7 demonstrates that the color coordinates values for the considered phosphors situate in the red region of CIE triangle. The color coordinate values for $\text{CaGd}_2\text{Si}_3\text{O}_{10}$ ($x = 0.56$, $y = 0.35$) are maximum and shifted more towards the ideal red region compared to the others. The CIE coordinates values are promising with PL results, demonstrating the highest intensity of $\text{CaGd}_2\text{Si}_3\text{O}_{10}:\text{Eu}^{3+}$ sample.

XRD INVESTIGATIONS

The diffraction investigations have been carried out to analyze crystal structure and phase purity of prepared materials. Figure 8a-d depicts the diffraction pattern of Eu^{3+} doped $\text{MGd}_2\text{Si}_3\text{O}_{10}$ ($M = \text{Mg}^{2+}$, Ca^{2+} , Sr^{2+} and Ba^{2+}) phosphors. In this type of host lattice, Eu^{3+} (95 pm) ion easily substitute Gd^{3+} (94 pm) ion because of the

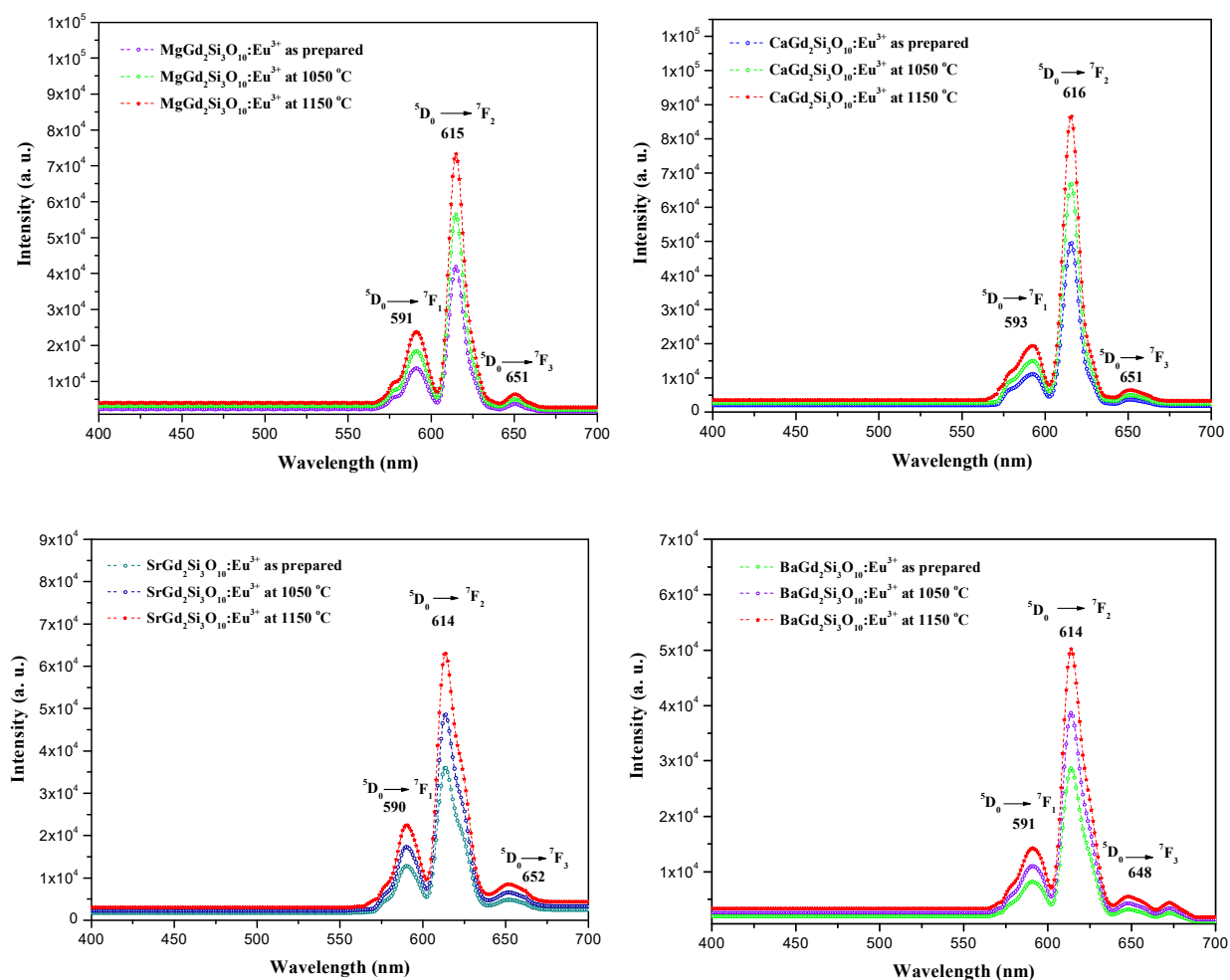


Figure 4. PL emission spectra for Eu(III) activated phosphors (a) $\text{MgGd}_2\text{Si}_3\text{O}_{10}$, (b) $\text{CaGd}_2\text{Si}_3\text{O}_{10}$, (c) $\text{SrGd}_2\text{Si}_3\text{O}_{10}$ and (d) $\text{BaGd}_2\text{Si}_3\text{O}_{10}$.

same valence and nearly similar size and hence gives rise to the diffraction patterns of $\text{MgGd}_2\text{Si}_3\text{O}_{10}$ type. Most intense peak for $\text{MgGd}_2\text{Si}_3\text{O}_{10}$ ($M = \text{Mg}^{2+}, \text{Ca}^{2+}, \text{Sr}^{2+}$ and Ba^{2+}) materials was observed to be at 32.24, 30.07, 31.63 and 28.84 two theta angles correspondingly. Influence of temperature on the crystallinity of phosphor materials is also perceived.

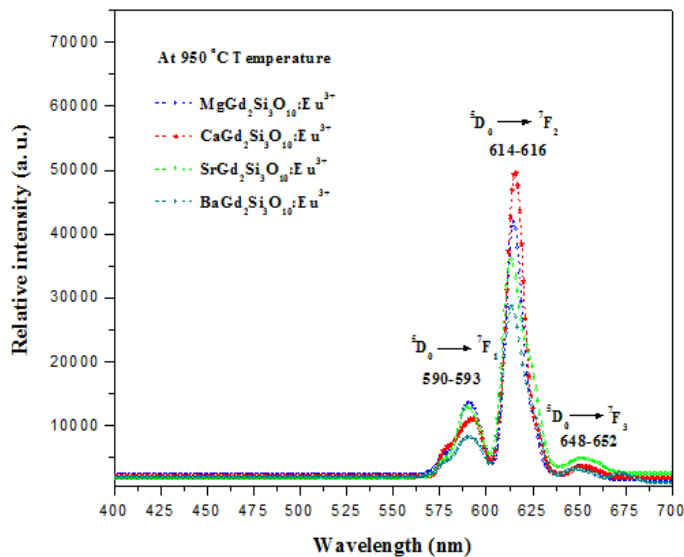


Figure 5. Relative PL emission spectra for europium(III) activated $\text{MgGd}_2\text{Si}_3\text{O}_{10}$ fluorescent materials at 950 °C.

Table 1. Various optical transitions, main peak and color corresponding to Eu^{3+} activated silicate materials.

Type of Lattice	$^5\text{D}_0 \rightarrow ^7\text{F}_1$	$^5\text{D}_0 \rightarrow ^7\text{F}_2$	$^5\text{D}_0 \rightarrow ^7\text{F}_3$	Intense Transition	Color
$\text{MgGd}_2\text{Si}_3\text{O}_{10}:\text{Eu}^{3+}$	591	615	651	615	Red
$\text{CaGd}_2\text{Si}_3\text{O}_{10}:\text{Eu}^{3+}$	593	616	651	616	Red
$\text{SrGd}_2\text{Si}_3\text{O}_{10}:\text{Eu}^{3+}$	590	614	652	614	Red
$\text{BaGd}_2\text{Si}_3\text{O}_{10}:\text{Eu}^{3+}$	591	614	648	614	Red

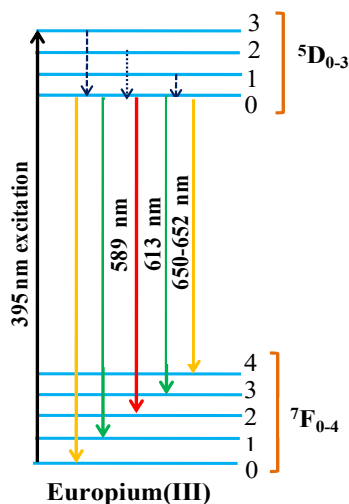


Figure 6. Diagram showing various energy states in Eu^{3+} ion and their transitions.

Table 2. CIE color coordinate values for Eu^{3+} activated $\text{MgGd}_2\text{Si}_3\text{O}_{10}$ nanophosphors at respective temperatures.

Type of Lattice	950 °C		1050 °C		1150 °C	
	x	y	x	y	x	y
$\text{MgGd}_2\text{Si}_3\text{O}_{10}:\text{Eu}^{3+}$	0.52	0.34	0.53	0.34	0.54	0.35
$\text{CaGd}_2\text{Si}_3\text{O}_{10}:\text{Eu}^{3+}$	0.54	0.35	0.55	0.35	0.56	0.35
$\text{SrGd}_2\text{Si}_3\text{O}_{10}:\text{Eu}^{3+}$	0.51	0.33	0.52	0.34	0.53	0.34
$\text{BaGd}_2\text{Si}_3\text{O}_{10}:\text{Eu}^{3+}$	0.50	0.33	0.51	0.34	0.52	0.34

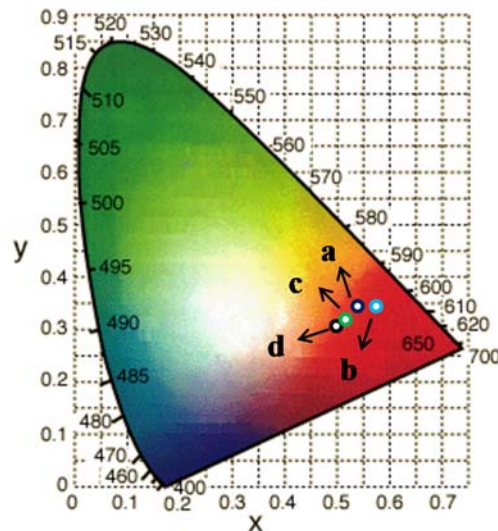


Figure 7. Color triangle demonstrating CIE coordinates synthesized phosphors at 1150 °C (a) $\text{MgGd}_2\text{Si}_3\text{O}_{10}$, (b) $\text{CaGd}_2\text{Si}_3\text{O}_{10}$, (c) $\text{SrGd}_2\text{Si}_3\text{O}_{10}$ and (d) $\text{BaGd}_2\text{Si}_3\text{O}_{10}$.

The intensity and crystallinity of the diffraction peaks gets enhanced with re-heating temperature. The variation of metal ions in the crystal lattice influences the structure of these phosphors. Change of alkaline earth metals ions ($M = \text{Mg}^{2+}/\text{Ca}^{2+}/\text{Sr}^{2+}/\text{Ba}^{2+}$) in $\text{MgGd}_2\text{Si}_3\text{O}_{10}$ lattice gives rise to the different diffraction pattern of these materials suggesting that they have different crystal structures. Debye Scherrer’s formula (I) have been applied to determine the size of particles of the considered phosphors.³⁸

$$D = k\lambda/\beta\cos\theta \quad \dots\dots\dots (I)$$

where D signifies particle size, k is the constant that depends on the shape of the particle, λ (1.5416 Å) stands for the X-ray wavelength, θ denotes incident Bragg’s angle and β signifies FWHM. The crystallite size of the as prepared $\text{MgGd}_2\text{Si}_3\text{O}_{10}$ having phosphors is summarized in Table 3.

TEM ANALYSIS

The morphological study together with shape, size and particles distribution was done by transmission electron microscopic analysis. Figure 9 shows the TEM images of the synthesized materials at 950 °C. TEM micrographs provide good precision on the crystal size of phosphor materials. Particle size of the prepared phosphors varied in the size from 15-25 nm having practical applicability in optoelectronic devices which are used in advanced display technologies. Nearly spherical shapes of particles are observed in the micrographs. $\text{MgGd}_2\text{Si}_3\text{O}_{10}$ exhibited well distinct

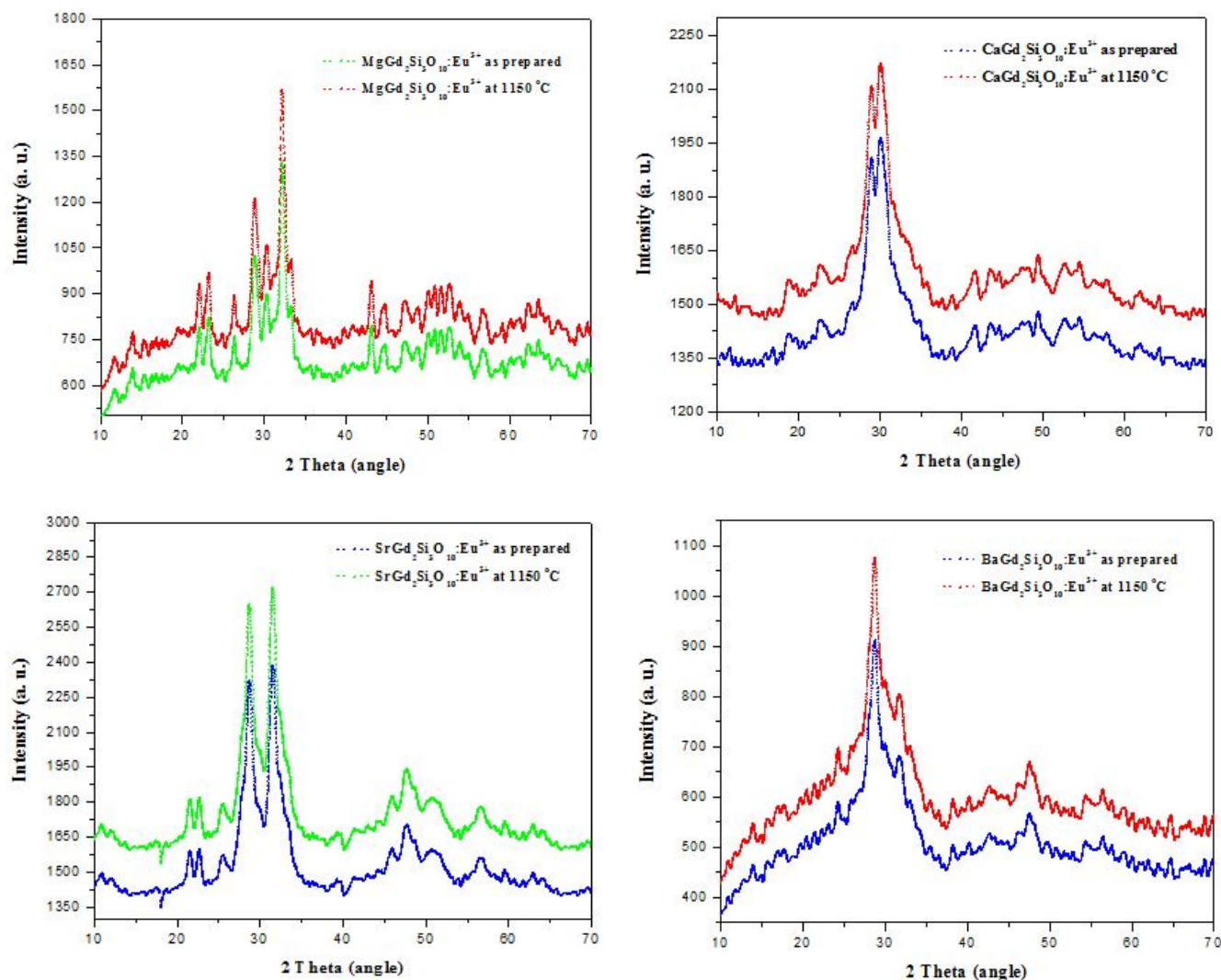


Figure 8. Diffraction profile of Eu^{3+} -doped $\text{MGd}_2\text{Si}_3\text{O}_{10}$ silicate phosphor material (a) $\text{MgGd}_2\text{Si}_3\text{O}_{10}$, (b) $\text{CaGd}_2\text{Si}_3\text{O}_{10}$, (c) $\text{SrGd}_2\text{Si}_3\text{O}_{10}$ and (d) $\text{BaGd}_2\text{Si}_3\text{O}_{10}$.

and nearly spherical shape of particles. $\text{CaGd}_2\text{Si}_3\text{O}_{10}$, $\text{SrGd}_2\text{Si}_3\text{O}_{10}$ and $\text{BaGd}_2\text{Si}_3\text{O}_{10}$ phosphor particles have irregular shape as revealed from their micrographs. The unbalanced distribution of the flow of mass and temperature during the synthesis of material is responsible for the abnormality in the shape and size of particles. Size of particles as estimated from TEM analysis is observed in good agreement with XRD investigations (Table 3).

Table 3. Particle size values investigated from diffraction data and TEM.

Type of Lattice	Particle size (TEM)	Particle size (XRD)
$\text{MgGd}_2\text{Si}_3\text{O}_{10}:\text{Eu}^{3+}$	15.14	12.56
$\text{CaGd}_2\text{Si}_3\text{O}_{10}:\text{Eu}^{3+}$	24.90	26.4
$\text{SrGd}_2\text{Si}_3\text{O}_{10}:\text{Eu}^{3+}$	15.14	26.8
$\text{BaGd}_2\text{Si}_3\text{O}_{10}:\text{Eu}^{3+}$	20.55	17.51

FTIR ANALYSIS

The FTIR spectra of sol-gel derived $\text{MGd}_2\text{Si}_3\text{O}_{10}$ materials were recorded in order to understand the structural properties and

different bonding modes of the phosphors. Figure 10a-d presents the FTIR spectrum of silicate phosphors recorded in $4000\text{--}400\text{ cm}^{-1}$ spectral range. In $\text{MgGd}_2\text{Si}_3\text{O}_{10}$, Mg-O stretching bond is strongly observed below 700 cm^{-1} wavenumbers. Absorption band located at 1066 cm^{-1} in $\text{MgGd}_2\text{Si}_3\text{O}_{10}$ phosphor relates to Si-O-Si mode of vibration. Si-O vibrations are located from $400\text{--}800\text{ cm}^{-1}$ region in these prepared materials. Si-O asymmetric stretching frequencies were reported in $1000\text{--}1300\text{ cm}^{-1}$ region, however, these peaks are centered at $1115, 1139, 1178\text{ cm}^{-1}$ in $\text{MgGd}_2\text{Si}_3\text{O}_{10}$, $\text{CaGd}_2\text{Si}_3\text{O}_{10}$ and $\text{BaGd}_2\text{Si}_3\text{O}_{10}$ phosphors. Absorption band at 706 and 1483 cm^{-1} in $\text{SrGd}_2\text{Si}_3\text{O}_{10}$ material corresponds to anti-symmetric vibrational frequency of the Sr-O bond in the structure.^{39,40}

In $\text{BaGd}_2\text{Si}_3\text{O}_{10}$ phosphor material, Gd-O vibration is centered at 492 cm^{-1} . Some peaks due to the nitrate precursors are also observed around 1427 and 1441 cm^{-1} in $\text{MgGd}_2\text{Si}_3\text{O}_{10}$ and $\text{BaGd}_2\text{Si}_3\text{O}_{10}$ materials. In $\text{Ba}_2\text{La}_2\text{Si}_2\text{O}_{10}$ silicate, absorption band at 855 cm^{-1} is owing to asymmetric vibrations of SiO^- in silicate tetrahedral unit. FTIR results are in good agreement with the XRD investigations. The shape of both XRD and FTIR differ with change in the alkaline earth metal (M) ions. The vibrations

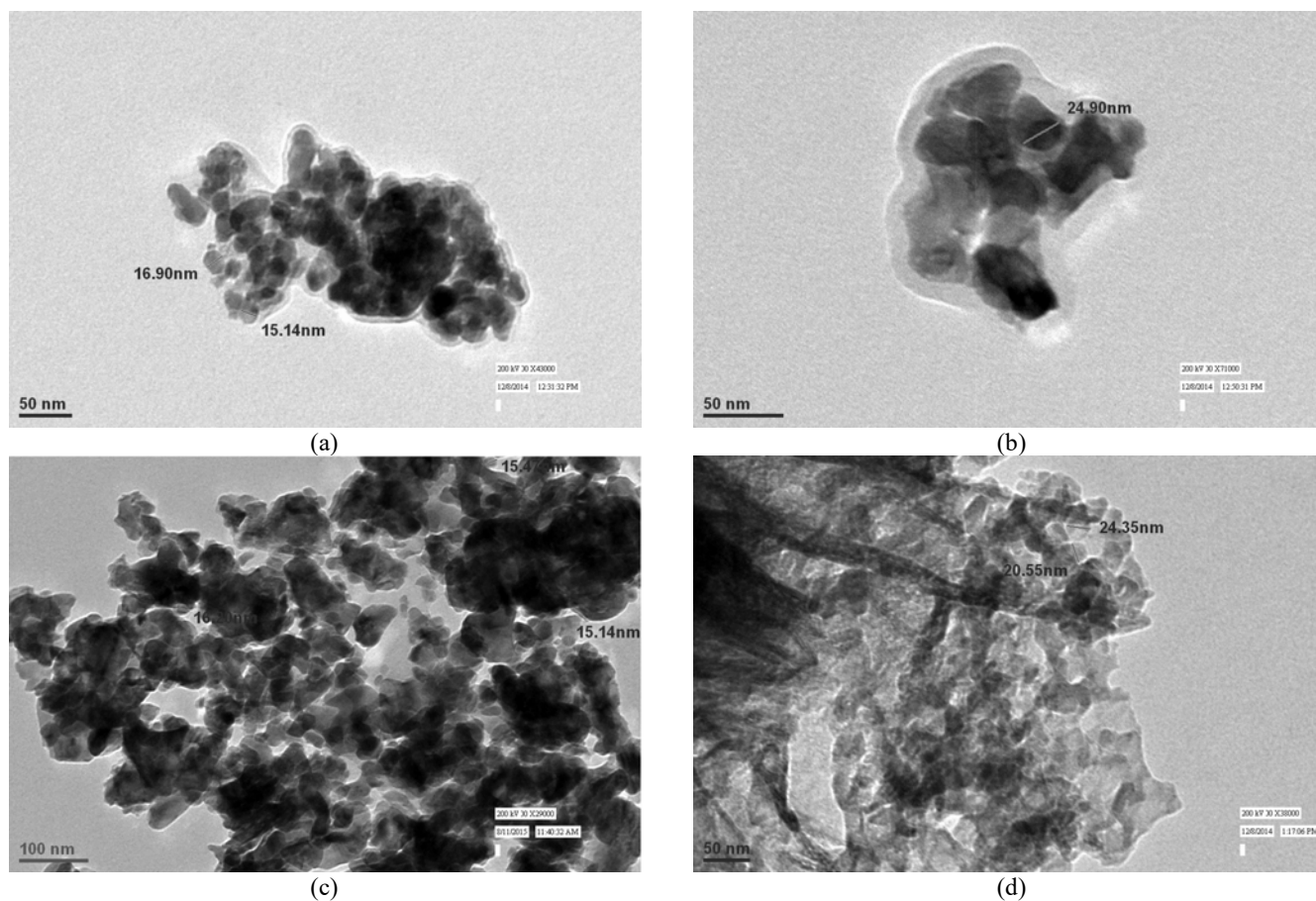


Figure 9. Transmission Electron Micrographs of Eu^{3+} doped silicate phosphors prepared at 950°C (a) $\text{MgGd}_2\text{Si}_3\text{O}_{10}$, (b) $\text{CaGd}_2\text{Si}_3\text{O}_{10}$, (c) $\text{SrGd}_2\text{Si}_3\text{O}_{10}$ and (d) $\text{BaGd}_2\text{Si}_3\text{O}_{10}$.

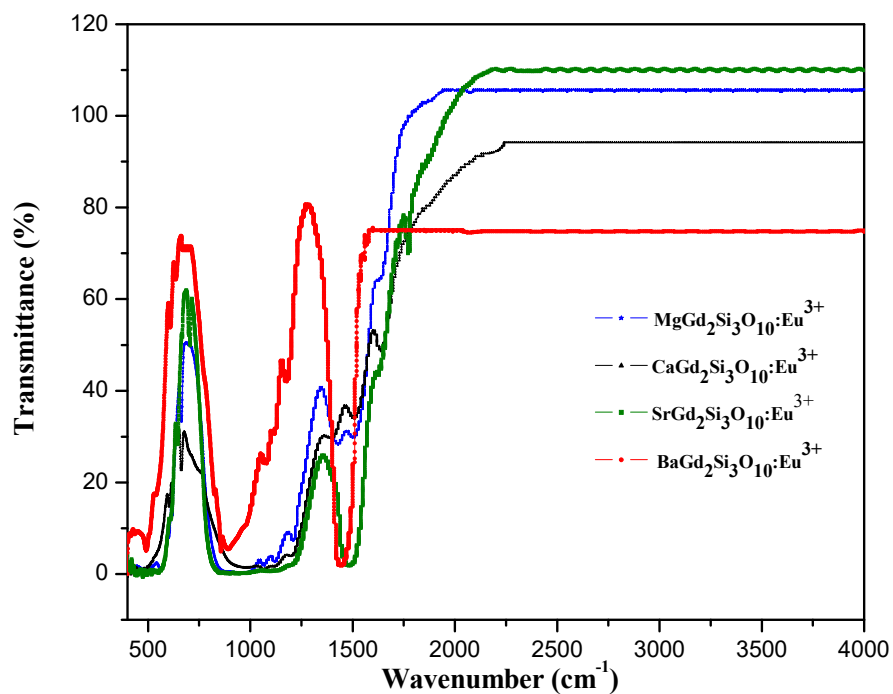


Figure 10 FTIR plots of Eu^{3+} doped $\text{MgGd}_2\text{Si}_3\text{O}_{10}$ phosphor prepared at 950°C (a) $\text{MgGd}_2\text{Si}_3\text{O}_{10}$, (b) $\text{CaGd}_2\text{Si}_3\text{O}_{10}$, (c) $\text{SrGd}_2\text{Si}_3\text{O}_{10}$ and (d) $\text{BaGd}_2\text{Si}_3\text{O}_{10}$.

corresponding to Si-O-Si, M-O, Gd-O and Eu-O bonds confirm the synthesis of Eu^{3+} doped $\text{MGd}_2\text{Si}_3\text{O}_{10}$ phosphors. The shape of both XRD and FTIR differ with change in the alkaline earth metal ions.

CONCLUSIONS

A rapid, easy and cost-effective sol-gel technique was applied for the fabrication of $\text{MGd}_2\text{Si}_3\text{O}_{10}:\text{Eu}^{3+}$ ($M = \text{Mg}^{2+}, \text{Ca}^{2+}, \text{Sr}^{2+}$ and Ba^{2+}) nanomaterials at 950 °C and their spectroscopic investigation were carried out. Photoluminescence characterization of the focused phosphors was strongly affected by the amount of Eu^{3+} ion and heating temperature used for material exploration. From the luminescence spectra of phosphors, it was found that 3 moles percent concentration of Eu^{3+} ion gave maximum photoluminescence response in the fabricated silicate phosphors. PL emission spectra of all the samples show deep red emission at 395 nm (excitation wavelength). The dominant emission peaks for these light emitting samples appears owing to $^5\text{D}_0 \rightarrow ^7\text{F}_2$ transition in 614-616 nm region. Maximum luminescence power of the phosphors was obtained when these materials were re-heated at 1150 °C. Structural studies revealed that these materials have improved crystallinity as the temperature raised up to 1150 °C. The structure and bonding of silicate phosphors analyzed by FTIR have found in concordance with XRD findings. TEM images have established that the considered nanosize of phosphor materials have a close agreement with diffraction analysis and have agglomerated crystal structure with nearly spherical shape of particles. Excellent PL emission intensity of these silicate phosphors demonstrates that the developed phosphors could have potential applications in modern display devices.

ACKNOWLEDGMENTS

Author (SS) acknowledge the financially viable provision from CSIR, New Delhi, India in the form of JRF [09/382(0194)/2017-EMR-1].

CONFLICT OF INTEREST STATEMENT

The authors declare that they have no conflict of interest.

REFERENCES AND NOTES

1. Y. Xiao, X.M. Chen, X.Q. Liu. Stability and microwave dielectric characteristics of $(\text{Ca}_{1-x}\text{Sr}_x)\text{LaAlO}_4$ ceramics. *J Electroceramics* **2008**, 21, 154-159.
2. B.S. Chhikara, R.S. Varma. Nanochemistry and nanocatalysis science: Research advances and future perspectives. *J Mat NanoSci* **2019**, 6, 1-6.
3. A. Patsha, S. Dhara, S. Chattopadhyay, K.H. Chen, L.C. Chen. Optoelectronic properties of single and array of 1-D III-nitride nanostructures: An approach to light-driven device and energy resourcing. *J Mat NanoSci* **2018**, 5, 1-22.
4. R.J. Xie, H.T. Hintzen. Optical properties of (oxy)nitride materials: A review. *J Am Ceram Soc* **2013**, 96, 665-687.
5. Y.C. Lin, M. Bettinelli, M. Karlsson. Unraveling the mechanisms of thermal quenching of luminescence in Ce^{3+} -doped garnet phosphors. *Chem Mater* **2019**, 31, 3851-3862.
6. D. Singh, V. Tanwar, A.P. Simantilke, B. Mari, P.S. Kadyan, I. Singh. Rapid synthesis and photoluminescent characterization of $\text{MAl}_2\text{O}_4:\text{Eu}^{2+}, \text{Dy}^{3+}$ ($M = \text{Ca}/\text{Ca} + \text{Ba}/\text{Ca} + \text{Mg}$) blue nanophosphors for white lighting display applications. *Adv Mater Lett* **2016**, 7, 47-53.

7. B. Liu, D. Ding, Z. Liu, F. Chen, C. Xia. Synthesis and electrical conductivity of various melilite-type electrolytes $\text{Ln}_{1+x}\text{Sr}_{1-x}\text{Ga}_3\text{O}_{7+x/2}$. *Solid State Ionics* **2011**, 191, 68-72.
8. H. Yu, X. Yu, X. Xu, T. Jiang, P. Yang, Q. Jiao, D. Zhou, J. Qiu. Excitation band extended in CaYAl_3O_7 : Tb^{3+} phosphor by Ce^{3+} co-doped for NUV light-emitting diodes. *Opt Commun* **2014**, 317, 78-82.
9. J. Singh, P.K. Baitha, J. Manam. Influence of heat treatment on the structural and optical properties of $\text{SrGd}_2\text{O}_4:\text{Eu}^{3+}$ phosphor. *J Rare Earths* **2015**, 33, 1040-1050.
10. F. Mo, L. Zhou, Q. Pang, Y. Lan, Z. Liang. Synthesis and luminescent properties of $\text{Zn}_{0.890}\text{Nb}_2\text{O}_6:\text{Eu}_{0.05}^{3+}, \text{Bi}_{0.005}^{3+}, \text{M}_{0.055}^{+}$ ($M = \text{Li}, \text{Na}, \text{K}$) phosphors. *Curr Appl Phys* **2013**, 13, 331-335.
11. I.P. Sahu, D.P. Bisen, N. Brahme, R.K. Tamrakar, R. Shrivastava. Luminescence studies of dysprosium doped strontium aluminate white light emitting phosphor by combustion route. *J Mater Sci: Mater Electron* **2015**, 26, 8824-8839.
12. M.R. Kadukar, P.W. Yawalkar, R. Choithrani, S.J. Dhoble. Mechnoluminescence, thermoluminescence, photoluminescence studies on $\text{Ca}_3\text{Y}_2\text{Si}_3\text{O}_{12}:\text{RE}^{3+}$ ($\text{RE}^{3+} = \text{Dy}^{3+}$ and Eu^{3+}) phosphors. *J Biolumin Chemilumin* **2015**, 30, 1219-1225.
13. J.K. Park K.J. Choi, H.G. Kang, J.M. Kim, C.H. Kim. Silicates phosphors for white LEDs identified through combinatorial Chemistry. *Electrochem Solid-State Lett* **2007**, 10, J15-J18.
14. D. Singh, S. Sheoran, J. Singh. Optical characterization of Eu^{3+} doped MLSIO_4 ($M = \text{Ca}, \text{Sr}, \text{Ba}$ and $L = \text{Mg}$) phosphor materials for display devices. *J Mater Sci: Mater Electron* **2018**, 29, 294-302.
15. D. Geng, G. Li, M. Shang, C. Peng, Y. Zhang, Z. Cheng, J. Lin. Nanocrystalline $\text{CaYAlO}_4:\text{Tb}^{3+}/\text{Eu}^{3+}$ as promising phosphors for full-color field emission displays. *Dalton Trans* **2012**, 41, 3078-3086.
16. Y. Yang, B. Liu, Y. Zhang, X. Lv, L. Wei, J. Xu, H. Zhang, X. Wang, C. Zhang, J. Li. Influence of $\text{Mg}^{2+}/\text{Ga}^{3+}$ doping on luminescence of $\text{Y}_3\text{Al}_5\text{O}_{12}:\text{Ce}^{3+}$ phosphors. *J Mater Sci: Mater Electron* **2018**, 29, 17154-17159.
17. A.K. Singh, S.K. Singh, S.B. Raia. Role of Li^+ ion in the luminescence enhancement of lanthanide ions: favorable modifications in host matrices. *RSC Adv* **2014**, 4, 27039-27061.
18. R.P. Rao. Preparation and characterization of fine-grain yttrium-based phosphors by sol-gel process. *J Electrochem Soc* **1996**, 143, 189-197.
19. E. Hertle, L. Chepyga, M. Batentschuk, L. Zigan. Influence of codoping on the luminescence properties of YAG:Dy for high temperature phosphor thermometry. *J Lumin* **2017**, 182, 200-207.
20. T. Ishigaki, H. Mizushima, U. Kazuyoshi, M. Nobuhiro, Y. Masahiro, T. Kenji, S. Mineo. Microwave synthesis technique for long phosphorescence phosphor $\text{SrAl}_2\text{O}_4:\text{Eu}^{2+}, \text{Dy}^{3+}$ using carbon reduction. *Materials Science and Engineering: B* **2010**, 173, 109-112.
21. L. Acosta, R. Puga, H. Loro, K.S. Gómez, J.M. Hernández, D. Acosta. Synthesis of LaF_3 inorganic nanoparticles: $\text{Er}^{3+}, \text{Yb}^{3+}$ by the coprecipitation method and characterization by optical spectroscopy and electron microscopy. *Journal of Physics: Conf. Series* **2018**, 1143, 1-8.
22. G. Zhu, M. Xie, Q. Yang, Y. Liu. Hydrothermal synthesis and spectral properties of Ce^{3+} and Eu^{2+} ions doped KMgF_3 phosphor. *Opt Laser Technol* **2016**, 81, 162-167.
23. Y.C. Kang, Y.S. Chung, S.B. Park. Preparation of $\text{YAG}:\text{europium}$ red phosphors by spray pyrolysis using a filter-expansion aerosol generator. *J Am Ceram Soc* **2004**, 82, 2056-2060.
24. D. Singh, S. Kadyan, S. Bhagwan. Structural and photoluminescence characteristics of $\text{M}_3\text{Al}_5\text{O}_{12}:\text{Eu}^{3+}$ ($M = \text{Y}, \text{Gd}$ and La) nanophosphors for optoelectronic applications. *J Mater Sci: Mater Electron* **2017**, 28, 13478-13486.
25. F. Xiao, Y.N. Xue, Q.Y. Zhang. Bluish-green color emitting $\text{Ba}_2\text{Si}_3\text{O}_8:\text{Eu}^{2+}$ ceramic phosphors for white light-emitting diodes. *Spectrochim Acta A Mol Biomol Spectrosc* **2009**, 74, 758-760.
26. M. Singh, S. Tlali. Effect of size on Debye temperature, melting entropy and enthalpy of nanomaterials. *J. Mater. Nanosci.* **2017**, 4 (1), 1-5.
27. Y. Zhang, J. Xu, B. Yang, Q. Cui, T. Tian. Luminescence properties and energy migration mechanism of Eu^{3+} activated $\text{Bi}_4\text{Si}_3\text{O}_{12}$ as a potential phosphor for white LEDs. *Mater Res Express* **2018**, 5, 1-8.

28. L. Tian, L. Wang, L. Zhang, Q. Zhang, W. Ding, M. Yu. Enhanced luminescence of Dy³⁺/Bi³⁺ co-doped Gd₃Al₅O₁₂ phosphors by high-efficiency energy transfer. *J Mater Sci: Mater Electron* **2015**, 26, 8507–8514.
29. B.R. Verma, R.N. Baghel. Structural and optical properties of Eu-doped silicate phosphors: A review. *Indian J Pure Appl Phys* **2017**, 13, 477–483.
30. D. Singh, S. Sheoran, V. Tanwar, S. Bhagwan. Optical characteristics of Eu(III) doped MSiO₃ (M = Mg, Ca, Sr and Ba) nanomaterials for white light emitting applications. *J Mater Sci: Mater Electron* **2017**, 28, 3243–3253.
31. J. Liao, S. Liu, B. Liu, L. Nie, J. Fu, H.R. We. Sol-gel preparation and photoluminescence properties of CaREAl₃O₇:Eu³⁺ (RE=Y, Gd, Lu) phosphors. *Optik - International Journal for Light and Electron Optics* **2015**, 126, 3781–3785.
32. X. Li, Y. Zhang, D. Geng, J. Lian, G. Zhang, Z. Hou, J. Lin. CaGdAlO₄:Tb³⁺/Eu³⁺ as promising phosphors for full-color field emission displays. *J Mater Chem C* **2014**, 2, 9924–9933.
33. H. Song, D. Chen. Combustion synthesis and luminescence properties of SrAl₂O₄:Eu²⁺, Dy³⁺, Tb³⁺ phosphor. *Luminescence* **2007**, 22, 554–558.
34. Z. Xia, D. Chen, M. Yang, T. Ying. Synthesis and luminescence properties of YVO₄:Eu³⁺, Bi³⁺ phosphor with enhanced photoluminescence by Bi³⁺ doping. *J Phys Chem Solids* **2010**, 71, 175–180.
35. H. Liu, Y. Hao, H. Wang, J. Zhao, P. Huang, B. Xu. Luminescent properties of R⁺ doped Sr₂SiO₄:Eu³⁺ (R⁺ = Li⁺, Na⁺ and K⁺) red-emitting phosphors for white LEDs. *J Lumin* **2011**, 131:2422–2426.
36. D. Singh, S. Sheoran. Synthesis and luminescent characteristics of M₃Y₂Si₃O₁₂:Eu³⁺ (M = Ca, Mg, Sr and Ba) nanomaterials for display applications. *J Mater Sci.: Mater Electron* **2016**, 27, 12707–12718.
37. X. Niua, J. Xua, Y. Zhanga, Y. Chua, B. Yanga, C. Zhang. Photoluminescence properties and concentration quenching of Dy³⁺ doped YAG phosphors for domestic lighting. *J Ceram Process Res* **2015**, 16, 609–613.
38. C.A. Rao, P.R.V. Nannapaneni, K.V.R. Murthy. Synthesis and luminescent properties of strontium cerium oxide phosphors doped with rare earths. *J Sci Res* **2013**, 5, 1–11.
39. R. Bala, A. Agarwal, S. Sanghi, S. Khasa. Influence of SiO₂ on the structural and dielectric properties of ZnO·Bi₂O₃·SiO₂ glasses. *J. Integr. Sci. Technol.* **2015**, 3 (1), 6–13.
40. I.P. Sahu, D.P. Bisen, N. Brahme, R.K. Tamrakar. Photoluminescence properties of europium doped di-strontium magnesium di-silicate phosphor by solid state reaction method. *J Radiat Res Appl Sci* **2015**, 8, 104–109.